The Chemical Enrichment History of the Small Magellanic Cloud and Its Gradients[1]

Ricardo Carrera[1], Carme Gallart and Antonio Aparicio[2]

Instituto de Astrofísica de Canarias, Spain

rcarrera@iac.es

carme@iac.es

Edgardo Costa and Rene A. Méndez

Departamento de Astronomía, Universidad de Chile, Casilla 36–D, Santiago, Chile

and

Noelia E. D. Noël

Instituto de Astrofísica de Canarias, Spain

ABSTRACT

We present stellar metallicities derived from Ca II triplet spectroscopy in over 350 red giant branch stars in 13 fields distributed in different positions in the SMC, ranging from $\sim 1^\circ$ to $\sim 4^\circ$ from its center. In the innermost fields the average metallicity is [Fe/H] ~ -1. This value decreases when we move away towards outermost regions. This is the first detection of a metallicity gradient in this galaxy. We show that the metallicity gradient is related to an age gradient, in the sense that more metal-rich stars, which are also younger, are concentrated in the central regions of the galaxy.

Subject headings: local group galaxies: evolution — galaxies: individual (SMC) — galaxies: stellar content — Magellanic clouds

[1]Currently at Osservatorio Astronomico di Bologna, Via Ranzani 1, I-40127 Bologna, Italy; ricardo.carrera@bo.astro.it

[2]Departamento de Astrofísica, Universidad de La Laguna, Spain

[1]Based on observations collected at the European Southern Observatory, Chile, within the observing programs 074.B-0446

1. Introduction

The chemical enrichment history of a galaxy is related to the origin and distribution of nuclear species in its stars and gas. The chemical elements are mainly produced by stars which drive the enrichment of the interstellar medium by ejecting material containing the product of the stellar nucleosynthesis from which the new generations of stars are formed. In addition, gas flows also play an important role in chemical enrichment, diluting the products of the stellar nucleosynthesis with unenriched material from outside the galaxy, and mixing metals from one part of the system to another (e.g. bringing metal-rich gas into metal-poor regions). Thus, the study of chemical evolution of galaxies involves understanding the spatial distribution and temporal evolution of various elements by taking into account the processes of star formation, the distribution of stars according to their masses and chemical compositions, and the final yields of various elements and detectable remnants of parent stars. Until recently, only the chemical enrichment history of the solar vicinity could be studied in detail. However, the modern multiobject spectrographers attached to the 8-10 m class telescopes allow us to study the chemical enrichment history of the nearest Local Group galaxies.

Because of their proximity, and the fact that they present a wide range of ages and metallicities, the Magellanic Clouds are attractive objects to study chemical enrichment histories. In a previous paper (Carrera et al. 2008, hereafter paper III), we investigated the chemical enrichment history of the LMC. In this paper, we will focus in the study of the SMC. There are considerable less studies of the SMC as compared with the LMC, probably due to: (i) its irregular appearance, with complex kinematics; (ii) its distance, located further away than the LMC; and (iii) its depth in the line of sight, which remains a subject of controversy.

Most of the information about the stellar populations of the SMC has been obtained from its cluster system (e.g. Da Costa & Hatzidimitriou 1998; Piatti et al. 2001, 2005). The cluster age distribution does not show the age-gap observed in the LMC (Da Costa & Hatzidimitriou 1998; Mighell, Sarajedini, & French 1998). From a sample of seven clusters older than 1 Gyr, Rich et al. (2000) suggest that star formation was stronger in two main episodes, one $\sim$8$\pm$2 Gyr ago and another $\sim$2$\pm$0.5 Gyr ago. However, there does not seem to be any age interval completely lacking of objects (Rafelski & Zaritsky 2005). There is only one old cluster, NGC 121, that is younger than most of the LMC globular clusters (Piatti et al. 2005). However, the SMC shows a significant old field population (Noël et al. 2007, hereafter Paper I).

To our knowledge, there are only three studies in which the star formation history (SFH) of the SMC field population was derived (Dolphin et al. 2001; Harris & Zaritsky 2004). From a deep color–magnitude diagram (CMD) Dolphin et al. (2001) found than the star formation in a small field in the periphery of this galaxy was relatively constant until about 2 Gyr ago,

with no star formation occurring since then. However, this could be biased by the fact that their field was specifically chosen because it did not have young stars. Harris & Zaritsky (2004) studied a $4^\circ \times 4.^\circ 5$ field in the central region of the galaxy. From shallower CMDs they found that the star formation in the SMC has had two main episodes: one which formed the oldest populations and lasted until 8.5 Gyr ago, and a recent one that started around 3 Gyr ago. Noël et al (2008, in preparation) have also obtained accurate SFHs for the fields presented in this paper, using CMDs reaching the oldest main sequence turnoffs with good photometric accuracy. They find that two main episodes of star formation in all fields, one at old ages ($\simeq$ 10 Gyr ago) and another one at intermediate ages ($\simeq$ 5 Gyr ago), in addition to young star formation in the wing fields.

Detailed determinations of chemical abundances exist only for the youngest population of the SMC (i.e. Hill, Barbuy, & Spite 1997; Venn 1999; Hunter et al. 2007), and its chemical enrichment history has been mainly determined from studies from its cluster system. The cluster age–metallicity relationship (AMR) has been obtained by Piatti et al. (2005) and Mighell, Sarajedini, & French (1998), mainly from photometric indicators. An initial chemical enrichment has been found, followed by a period of relatively slow increase in the metal abundance. Clusters more metal-rich than [Fe/H]$\geq$-1 are younger than 5 Gyr. Since then, the metallicity has again increased until now. On average, the SMC is more metal-poor than the LMC. The very recent work by Idiart, Maciel & Costa (2007), which have obtained chemical abundances in a sample of SMC planetary nebulae, has found a similar result, with the exception that the chemical enrichment episode at a very early epoch is not observed.

In the present work we focus on obtaining stellar metallicities of individual red giant branch (RGB) stars in the field population of the SMC from Ca II triplet (hereafter CaT) spectroscopy. These stars have been selected in 13 fields distributed at different positions in the SMC ranging from $\sim 1^\circ$ to $\sim 4^\circ$ from its center. Deep photometry of these fields has been presented in Paper I . The procedure followed to select the targets is explained in Section 2. The data reduction is discussed in Section 3. The radial velocities of the stars in our sample are obtained in Section 4. In Section 5 we discuss the calculation of the CaT equivalent widths and the determination of metallicities. Section 6 presents the method used to derive ages for each star by combining the information on their metallicity and position on the CMD. The analysis of the data is presented in Section 7. The metallicity distribution of each field and the possible presence of a metallicity gradient is discussed in Section 7.1. The derived AMRs for each field are presented in Section 7.2. The main results of this paper are discussed in Section 8.

2. Target Selection

In the framework of a large program to obtain proper motions, deep CMDs and stellar metallicities in the SMC, we secured spectroscopy of stars in 13 fields spread about the galaxy body. The photometry of these fields, presented in Paper I and listed in Table 1, were obtained with a Tektronic 2048×2048 CCD detector attached to the LCO 100″ telescope, which covers a field size of 8.′85× 8.′85. Following the notation described by Tinney, Da Costa & Zinnecker (1997), fields denoted by "qj" (followed by right ascension) are centered on quasars and were observed photometrically with the main objective of determining the absolute proper motion of the SMC (Costa et al., in preparation). Fields labeled "smc" were selected specifically to study their stellar populations by sampling a range of galactocentric radius at similar azimuth. The BR photometry of these fields is described in detail in Paper I, where the distribution of stellar populations of the SMC is discussed on the basis of CMDs. These observations have been complemented with observations in the I band in order to allow using the reduced equivalent width-metallicity (W'$_I$-[Fe/H]) relationship derived in Carrera et al. (2007, hereafter Paper II) to obtain metallicities for individual RGB stars. I–band observations of "qj" fields were obtained with the same instrument and telescope as the BR photometry. The I images of "smc" fields were obtained with FORS2 at the VLT in image mode and were also used for spectroscopic mask configuration of MXU@FORS2. Field qj0111 was observed with both telescopes in order to compare the photometric calibrations. The magnitudes obtained with each calibration differ by about ∼0.1 magnitudes. This relatively large difference is mainly explained by the poor photometric calibration of the FORS2 images, which were not taken for photometric purposes. In any case, this error means a metallicity uncertainty of only ∼0.02 dex, a value smaller than the metallicity uncertainty itself (∼0.1 dex).

In each field we selected stars in two windows of the CMD, which are plotted in Figure 1. In each region the stars were ordered from the brightest to the faintest ones, regardless of their color. The resulting star list was used as input for the mask configuration task of the instrument. Stars in the box below the RGB tip were given higher priority, and only objects above the tip were observed when it was impossible to put the slit on a star of the lower region.

3. Observations and Data Reduction

The spectroscopic observations were carried on in service mode with the VLT ANTU telescope, at Paranal Observatory (Chile), through program 074.B-0446. We used FORS2 in MXU multiobject mode with grism 1028z+29 and filter OG590+32 in order to eliminate

residual orders. Slits with a length of 8″ and a width of 1″ were selected. With this setup, we were able to observe about 40 objects in each field (the final number depends on the spatial distribution of the selected stars). The slit length was selected with the purpose of shifting the stars along it in order to acquire two exposures of each field without superposition of the stellar spectra in each. This particular procedure allowed to extract the spectra in the same way as Paper II.

After bias subtraction, each image was flat-field corrected. Then, as each star is in a different position in the two images of the same field, we subtracted one from the other, obtaining a positive and a negative spectrum of the same star. With this procedure the sky is subtracted in the same pixel in which the star has been observed, thus, minimizing the effects of pixel-to-pixel sensitivity variations. Sky residuals due to temporal variation of the sky brightness were eliminated in the following step, in which the spectrum is extracted in the usual way and the remaining sky background is subtracted using the information on both sides of the stellar spectrum. In the next step, the spectra were wavelength calibrated and added to obtain the final spectrum. Finally, each spectrum was normalized by fitting a polynomial, excluding the strongest lines (such as the CaT lines). There is an uncertainty in the wavelength calibration because the arcs used for this purpose were not taken at the same time and with the same telescope pointing as the object. The effects of this on the wavelength calibration have been discussed by Gallart et al. (2001). Since we are not interested in obtaining precise radial velocities, this problem will not significantly affect our results.

In total, we observed 386 stars in the 13 SMC fields. Their magnitudes and CaT equivalent widths are listed in Table 2

4. Radial Velocities

The radial velocity of each star was calculated in order to reject SMC non-members. We used the IRAF *fxcor* task, which performs the cross-correlation between the target and template spectra of stars of known radial velocity (Tonry & Davis 1979). As templates we selected nine stars in the clusters NGC 104, NGC 2682, NGC 288 and NGC 7078 which were observed within the same program as the SMC fields and presented in Paper II. The velocities were corrected to the heliocentric reference frame within *fxcor*. The final radial velocity for each SMC star is the average of the velocities obtained from each template, weighted by the width of the corresponding correlation peaks. The resulting velocities can be affected by the fact that the stars might have not been positioned exactly in the center of the slit. The importance of this is described in detail in Paper II. However, in the case

of the SMC, the stars were observed at a relatively large air mass ($\geq$1.6) and with a seeing near to or larger than 1″. Since the slit width was 1″, the effect of the incorrect centering of the star on the slit was of little importance. In fact, when we tried to characterize this effect in the way described in Paper II, we found that its contribution to the resulting velocity is smaller than the uncertainty due to the wavelength calibration. For this reason, we did not take this effect into account in the final radial velocity. We considered as SMC members those stars with radial velocities in the range $50 \leq V_r \leq 250$ km s^{-1} (Harris & Zaritsky 2006).

5. CaT Equivalent Widths and Metallicity determination

The metallicity of the RGB stars is obtained following the procedure described in Paper II. The equivalent width is the area of the line normalized to the local continuum within a line bandpass. The continuum is calculated from a linear fit to the mean value of the corresponding bandpasses. The line and continuum bandpasses used in this work are listed in Table 3. The line flux is calculated from the fit of its profile using a Gaussian plus a Lorentzian function. As discussed in Paper II, this function provides a better fit to the core and the wings of the strongest lines than other functions previously used. The CaT index, denoted as ΣCa, is defined as the sum of the equivalent widths of the three CaT lines. The ΣCa and their uncertainties for each star observed are given in Table 2, together with their magnitudes and radial velocities. Two calibrations of the CaT as metallicity indicator were obtained in Paper II based on I and V magnitudes. In this case, only I magnitudes are available for the SMC stars. The reduced equivalent width, W'$_I$, for each star has been calculated using the slope obtained in Paper II for the calibration clusters in the M_I-ΣCa plane (β_I=-0.611 Åmag^{-1}). To obtain the absolute magnitudes we assumed a distance modulus of $(m\text{-}M)_0$=18.9 (see van den Bergh 1999) and reddenings listed in the last column of Table 1 (see Paper I for details). Also, in Paper II three different metallicity scales were used as reference. In this case, we only used the relationships obtained on the Carretta & Gratton (1997, hereafter CG97) metallicity scale, because it is the only one that uses homogeneous high-resolution metallicities of open and globular clusters, and because the metallicities of the LMC stars in Paper III were also obtained in this way.

In brief, the metallicity for each star is given by:

$$[Fe/H]_{CG97} = -2.95 + 0.38\Sigma Ca + 0.23 M_I \quad (1)$$

In Figures 2, 3 and 4 the position of SMC stars (radial velocity members) in the M_I-ΣCa plane for our eastern, western, and southern fields, are respectively shown. Solid lines

indicate the magnitude range of the observed cluster stars used in Paper II to obtain the above relationship. Dashed lines show the region where the relationship is extrapolated.

The metallicity distribution of each field is shown in Figures 5, 6 and 7 and will be discussed in Section 7.1.

6. Determination of stellar ages

The position of the RGB on the CMD suffers from age–metallicity degeneracy. However, when the metallicity is obtained in an alternative way, as in this case from spectroscopy, this age–metallicity degeneracy can be broken, and ages can be derived from the position of the stars in the CMD. In paper III, a polynomial relationship was computed to derive stellar ages from their metallicities and positions in the CMD. For that purpose, synthetic CMDs computed with IAC-star (Aparicio & Gallart 2004) with the overshooting BaSTI (Pietrinferni et al. 2004) and Padova (Girardi et al. 2002) stellar stellar evolution models as input were used. As it is explained in Paper III, differences between both models in the resulting ages are negligible for our purpose, since we are not interested in an accurate determination of ages. For simplicity, as in Paper III, we used only the relationship obtained from the BaSTI stellar models. The aforementioned relation was obtained for $(V-I)$ and M_V. Since V magnitudes are unavailable for our sample of SMC stars, we computed a new relationship for B, R, and I magnitudes. In this case, we selected $(B-I)$ instead of $(B-R)$ because the former is much more sensitive to small changes in the stellar metallicity and age.

We followed the same procedure as in Paper III. First, we used the same synthetic CMD used in Paper III [2], which was computed with a constant star formation rate (SFR) between 0 and 13 Gyr and with a chemical law such that any star can have any metallicity between -2.3 to $+0.5$ dex. In this CMD we only selected stars in the same region below the tip of the RGB in which the observed ones were mainly chosen. We did not consider the brightest AGB stars due to the uncertainty of their parameters as predicted by stellar evolution models. Following the same statistical procedure described in Paper III, we checked which polynomial combinations of magnitude M_I, color $(B-I)$ and metallicity $[Fe/H]$ best represent the age

[2]During the referreing process of this paper, the authors of the BaSTI models discovered a problem in the calculation of models in the mass range 1.1–2.5 $M_\odot$ ($\simeq$1–4 Gyr), (see http://albione.oa-teramo.inaf.it/). Even though the differences between the new and old models were unlikely to affect in any substantial way our results, we recalculated equation 2 using a synthetic CMD computed with the updated model set. All the results shown are derive from this new relationship. We have verified that the differences are indeed minor, and that, therefore, the results on the LMC on paper III, obtained using the faulty models, can be trusted nevertheless.

of the stars in this synthetic CMD. In order to minimize the σ and to improve the correlation coefficient, different linear, quadratic and cubic terms of each observed magnitude have been added. We have checked whether M_I or M_B magnitudes improve the relationship. Similar results are obtained for both magnitudes, so we choose the first because metallicities were calculated from it. The final polynomial form adopted is:

$$log(age) = a + b(B-I) + cM_I + d[Fe/H] + f(B-I)^2 + g[Fe/H]^2 \quad (2)$$

The best fit coefficients are listed in Table 4.

In order to estimate the age uncertainty when this relationship is used to compute stellar ages, we performed a Monte Carlo test as in paper III. The goal is to check how the obtained ages change when the input parameters are modified. The test consists in computing, for each synthetic star, several age values for stochastically varying $[Fe/H]$, $(B-I)$ and M_I according to a gaussian probability distribution of the corresponding σ ($\sigma_{[Fe/H]}$ ∼0.15 dex; $\sigma_{(B-I)}$ ∼0.001 and $\sigma_{M_I} \sim 0.001$). The σ value of the obtained ages provide an estimation of the age error when Equation 2 is used. The obtained values for the considered age intervals are shown in Figure 8. The age uncertainty increases for older ages.

It is also necessary to check how well equation 2 reproduces the age of a real stellar system. Following the same steps as in Paper III, we choose the cluster stars used in Paper II for the calibration of the CaT as metallicity indicator. For those stars we knew their $(B-I)$ color and M_I magnitudes, so we can compute their metallicity in the same way as was done for the SMC stars (see Section 5). We then used these observational magnitudes as input for equation 2, obtaining an age for each cluster star. The cluster age was computed as the mean of the ages of its member stars. In Figure 9, the age computed for each cluster has been plotted versus its reference value. As in Paper III, ages younger than 10 Gyr are well recovered. However, the relationship saturates for ages larger than 10 Gyr.

7. Analysis

7.1. Metallicity distribution

Metallicity distributions are shown in Figures 5, 6 and 7 for eastern, western and southern SMC regions respectively. We have fitted a Gaussian to obtain the mean metallicity and metallicity dispersion of each of them. These values are listed in columns 3 and 4 of Table 5. The fields are ordered by its distance to the center, which is shown in column 2. Fields in different regions are indicated by different font types: eastern fields in normal, western fields

in boldface and southern fields in italics. Mean metallicities are very close to [Fe/H]$\sim$-1 in all fields within r$\lesssim$2.°5 from the SMC center. A similar value is observed for the southern fields up to r$\lesssim$3° (qj0047 and smc0049). Note that the SMC isopleths of intermediate–age and old stars are elongated in the NE-SW direction (PA=45°; Cioni, Habing & Israel 2000) and that a radius of 3° in the southern direction correspond to approximately the same isopleth at radius 2.°5 in the eastern and western directions. For the outermost fields, qj0033 in the West, and qj0102 and qj0053 in the South, the mean value is clearly more metal-poor than in the others.

The fact that the mean metallicity decreases when we move away from the center implies that there is a metallicity gradient in the SMC. This gradient is more clear when we compute the percentage of stars in different metallicity bins, values also listed in Table 5 (columns 5 and 6). For the western and southern fields, the percentage of stars more metal-poor than [Fe/H] = -1 increases when we move away from the center. This is not observed in the eastern fields because they are almost at the same distance. This is the first time that a metallicity gradient has been reported in SMC stellar populations. The detection of this gradient has been possible because we have covered a large radius range, up to 4° from the SMC center.

7.2. Age–metallicity relationships

From a purely phenomenological point of view, there are two main ways to account for the mean metallicity gradient found in the previous section. One possibility is that chemical enrichment has proceeded more slowly towards the SMC periphery, in such a way that coeval stars would be more metal-poor when we move away from the center. This seems to be the case of spiral galaxies, like the Milky Way, where the observed abundance gradients may be explained by radial variations of the relation between the SFR and the amount of infalling gas (e.g. Prantzos & Boissier 2000; Chiappini, Matteucci & Romano 2001). The situation would be complicated in dwarf galaxies by the probable existence of galactic winds originated in supernova explosions (e.g. Romano, Tosi & Matteucci 2006) which are able to remove large amount of metals from the interstellar medium. An alternative scenario is that the stellar AMR (i.e. the law of chemical enrichment as a function of time) has been the same everywhere in the SMC. As a result, the average metallicity of coeval stars would be the same in all fields and the metallicity gradient would be related to an age gradient. A mixture of both scenarios is also possible.

To investigate the nature of the gradient, we have therefore calculated the AMR for each field. They are plotted in Figures 10, 11, and 12 for fields situated to the East, West

and South respectively. Note that the uncertainty in age is much larger than in metallicity. However, as we are interested in the global behavior and not in obtaining individual stellar ages, the age determinations are still valid. Since the procedure to obtain the age saturates for values older than 10 Gyr, we can only be confident that the oldest stars have an age $\geq$ 10 Gyr. For these we assume an age of 12.9 Gyr, which is the age of the oldest cluster in the Milky Way (NGC 6426, Salaris & Weiss 2002). Regarding the youngest stars, in the region of the CMD where we selected the observed stars, and according to the stellar evolution models, we do not expect to find stars younger than $\sim$0.8 Gyr. However, equation 2 can formally compute ages younger than this value. As the age determination uncertainty for these young stars is $\sim$1 Gyr, in order to avoid this contradiction we assign them an age of 0.8 Gyr. Inset panels show the age distribution of the observed stars, with and without taking into account the age uncertainty (*solid line and histogram*, respectively). To obtain the first one, we assumed that the age of each star is represented by a Gaussian probability distribution on the age axis, with a mean value equal to the age calculated for this given star, and σ equal to the age uncertainty. The area of each of these distributions is unity. In the case of stars near the edges, the wings of the distribution may extend further than the limits. We have proceeded in the same way as described in Paper III, cutting off the wings outside the assumed limits (0.8 and 12.9 Gyr) and rescaling the rest of the distribution so that the area remains unity.

All the AMR plotted in Figures 10, 11 and 12 show a rapid chemical enrichment at a very early epoch. Even though in some fields we have not observed enough old stars to sample this part of the AMR, note that 12 Gyr ago all fields have reached [Fe/H]$\simeq -1.4$— -1.0. This initial chemical enrichment was followed by a period of very slow metallicity evolution until around 3 Gyr ago. Then, the galaxy started another period of chemical enrichment, which is observed in the innermost fields, which are, however,the only ones where we observed enough young stars to sample this part of the AMR. For a given age, the mean metallicity of the stars in fields qj0111, qj0112 and smc0057 seems to be slightly more metal-poor than those of other fields. The uncertainties in the age determination could account for the observed differences. In all cases, however, the mean metallicity is similar to that of the other fields at similar galactocentric radii. The field AMRs obtained in this work are similar to those for clusters (the reader should take into account that differences in the metallicity scales exist among different works), although there is only one cluster older than 10 Gyr (see Figure 13), and for planetary nebulae, with the exception that in these objects it is not observed the chemical enrichment episode at a very early epoch (see Figure 6 of Idiart, Maciel & Costa 2007).

It does not seem that there was a period in which the galaxy has not formed stars, in agreement with the result found in Paper I. (Figures 10, 11 and 12, inset panels). For eastern

fields, located in the wing, most of the observed stars have ages younger than 8 Gyr, but there is also a significant number of objects older than 10 Gyr. At a given galactocentric distance, eastern fields show a large number of young stars ($\leq$3 Gyr) in comparison to the western ones, as discussed in Paper I. For the western and southern fields, the fraction of intermediate-age stars, which are also more metal-rich, decreases as we move away from the center, although the average metallicity in each age bin is similar. This indicates the presence of an age gradient in the galaxy, which may be the origin of the metallicity one. It is noticeable that for the most external fields, qj0033 and qj0053, we find a predominantly old and metal-poor stellar population.

We can check statistically the hypothesis that the AMR is independent of the position in the SMC. To do so, we have combined the measurements on the 13 fields to obtain a global AMR and compared it with that of each field. To do so, we have divided the age range into six intervals (age<1.5 Gyr, 1.5–3.5 Gyr, 3.5–5.5 Gyr, 5.5–8.5 Gyr, 8.5–11 Gyr, >11 Gyr). We have computed the dispersion and mean metallicity in each age bin, and listed the results in Table 6. With these data, we have performed a χ^2 test as follows:

$$\chi^2 = \sum_{i=1}^{6} \frac{(Z_i^{field} - Z_i^{global})^2}{\sigma_i^2} \tag{3}$$

where σ_i^2 is the squared sum of the uncertainties in the age bin i of each field and the global AMR. The result is shown in Column 8 of Table 6. All fields, except qj0047 and smc0033, have values of χ^2_ν smaller than 1. The discrepancy in fields qj0047 and smc0033 may be due to small number statistics: there are only two stars younger than 11 Gyr in field qj0047 and three in smc0033. Values of χ^2_ν <1 mean that the observed AMR for each field is the same as the global one with a confidence of 90% (95% in most cases). From these results, we may conclude that the hypothesis that the AMR is independent of position is correct within the uncertainty.

8. Summary and Discussion

Using CaT spectroscopy, we have derived stellar metallicities for a large sample of RGB field stars in 13 regions of the SMC situated at different galactocentric distances and positions angles. We have found a radial metallicity gradient, which is most evident for those fields situated toward the South, where we covered a large galactocentric radius. For a given galactocentric distance, the mean metallicities for fields situated at different position angles are very similar. The inner fields have a mean metallicity of [Fe/H] ~ -1, which is similar

to that of the cluster metallicity distribution.

We have obtained the AMR of each field from the combination of metallicities, derived from CaT spectroscopy, and the position of stars in the CMD. All fields have similar AMRs, which are also similar to the clusters one (Piatti et al. 2005). All show a rapid initial increase of metallicity, followed by a very slow chemical enrichment period. A new relatively fast chemical enrichment episode is observed in the last few Gyrs in the fields within $\sim 2^{\circ}$ of the center with enough young stars to sample it. From the information on the AMRs, we conclude that coeval stars have the same metallicity everywhere in the SMC. The observed metallicity gradient is therefore related to an age gradient, because the youngest stars, which are also the most metal-rich, are concentrated in the central regions of the galaxy.

In a forthcoming paper we will try to reproduce the observed AMR with chemical evolution models using accurate SFRs, as a function of time, which are being derived by our group in each field (Noël et al. 2008, in preparation).

AA, CG, NEDN and RC acknowledge the support from the Spanish Ministry of Science and Technology (Plan Nacional de Investigación Científica, Desarrollo, e Investigación Tecnológica, AYA2004-06343). RC also acknowledges the funds by the Spanish Ministry of Science and Technology under the MEC/Fullbright postdoctoral fellowship program. EC and REM acknowledge support from the Fondo Nacional de Investigación Científica y Tecnolóliga (proyecto No. 1050718, Fondecyt) and from the Chilean Centro de Astrofísica FONDAP No. 15010003. This work has made use of the IAC-STAR Synthetic CMD computation code. IAC-STAR is supported and maintained by the computer division of the Instituto de Astrofísica de Canarias.

Facilities: VLT(FORS2).

REFERENCES

Aparicio, A., & Gallart, C. 2004, A&A, 128, 1465

Carrera, R., Gallart, C., Pancino, E. & Zinn, R. 2007, AJ, 134, 1298. Paper II

Carrera, R., Gallart, C., Hardy, E., Aparicio, A. & Zinn, R. 2008, AJ, 135, 836. Paper III

Carretta, E., & Gratton, R. G. 1997, A&AS, 121, 95. CG97

Chiappini, C., Matteucci, F., & Romano, D. 2001, ApJ, 554, 1044

Cioni, M. R. L., Habing, H. J., & Israel, F. P. 2000, A&A, 358, L9

Da Costa, G. S. & Hatzidimitriou, D. 1998, AJ, 115, 1934

Dolphin, A. E., Walker, A. R., Hodge, P. W., Mateo, M., Olszewski, E. W., Schommer, R. A. & Suntzeff, N. B. 2001, ApJ, 562, 303

Gallart, C., Martínez-Delgado, D., Gómez-Flechoso, M. A., & Mateo, M. 2001, AJ, 121, 2572

Girardi, L., Bertelli, G., Bressan. A., Chiosi, C., Groenewegen, M: A. T., Marigo, P., Salasnich, B., & Weiss, A. 2002, A&A, 391, 195

Harris, J. & Zaritsky, D. 2004, AJ, 127, 1531

Harris, J. & Zaritsky, D. 2006, AJ, 131, 2514

Hill, V., Barbuy, B. & Spite, M. 1997, A&A, 323, 461

Hill, V. 1999, A&A, 345, 430

Hunter, I., Dufton, P. L., Smartt. S. J., Ryans, R. S. I., Evans, C. J., Lennon, D. J., Trundle, C., Hubeny, I. & Lanz, T. 2007, A&A, 466, 277

Idiart, T. P., Maciel, W. J. & Costa, R. D. D. 2007, A&A, 472, 101

Mighell, K. J., Sarajedini, A. & French, R. S. 1998, AJ, 116, 2395

Noël, N. E. D., Gallart, C., Costa, E. & Méndez, R.A. 2007, AJ, 133, 2037 Paper I

Piatti, A. E., Santos, J. F. C., Clariá, J. J., Bica, E., Sarajedini, A. & Geisler, D. 2001, MNRAS, 325, 792

Piatti, A. E., Sarajedini, A., Geisler, D., Seguel, J., & Clark, D. 2005, MNRAS, 358, 1215

Piatti, A. E., Sarajedini, A., Geisler, D., Gallart, C., & Wischnjewsky, M. 2007, MNRAS, 382, 1202

Pietrinferni, A., Cassisi, S., Salaris, M., & Castelli, F. 2004, ApJ, 612, 168

Prantzos, N., & Boissier, S. 2000, MNRAS, 313, 338

Rafelski, M. & Zaritsky, D. 2005, AJ, 129, 2701

Rich, R. M., Shara, M., Fall, S. M. & Zurek, D. 2000, AJ, 119, 197

Romano, D., Tosi, M., & Matteucci, F. 2006, MNRAS, 365, 759

Salaris, M., & Weiss, A. 2002, A&A, 388, 492

Tinney, C. G., Da Costa, G. S. & Zinnecker, H. 1997, MNRAS, 285, 111

Tonry, J., & Davis, M. 1979, AJ, 84, 1511

van den Bergh, S. 1999, A&A Rev., 9, 273

Venn, K. A. 1999, ApJ, 518, 405

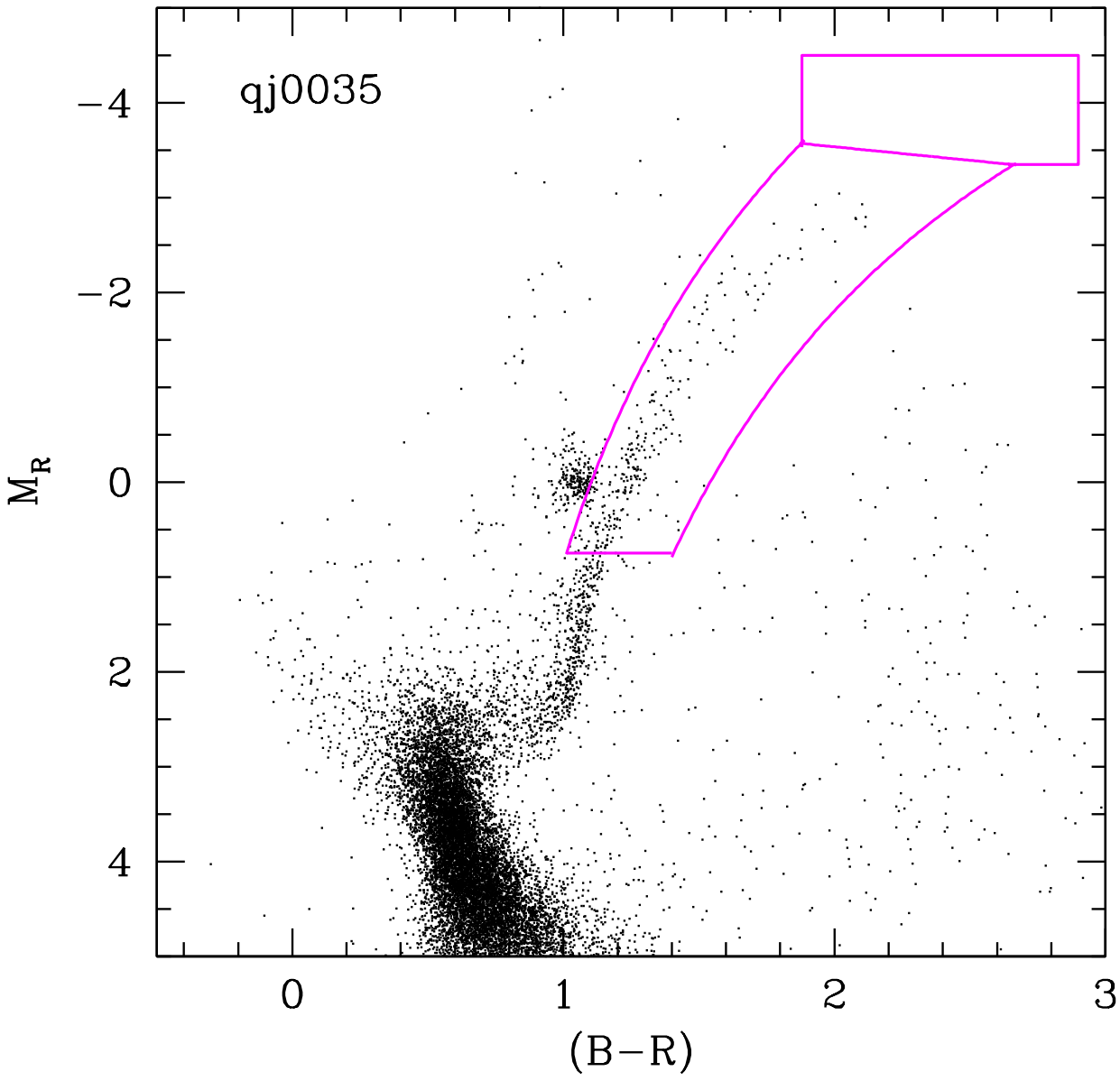

Fig. 1.— Color–magnitude diagram of the field qj0035 showing the RGB windows used to select the candidates to be observed spectroscopically.

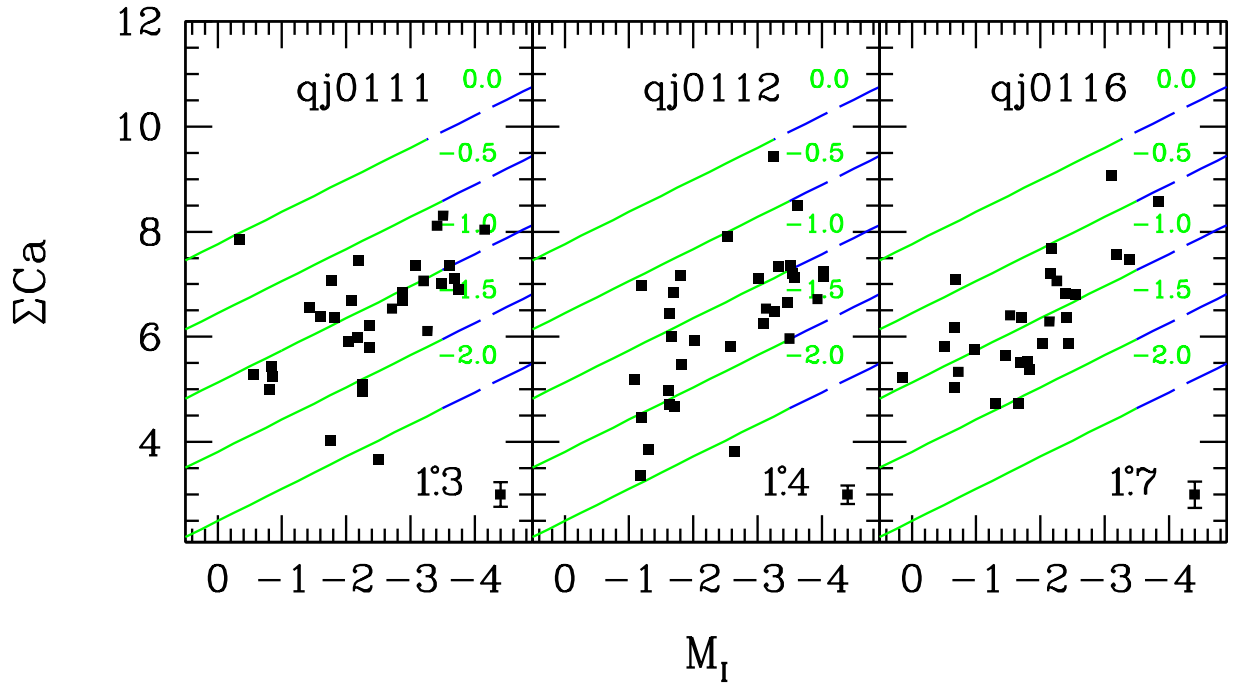

Fig. 2.— Position in the M_I–ΣCa plane of observed SMC stars in the eastern fields. Only stars with confirmed membership from their radial velocity are represented. The typical ΣCa error is shown in the bottom right corner of each panel. Isometallicity lines, obtained from the relationship based on M_I presented in Paper II, have been plotted for reference. The solid part of the line is the magnitude interval covered by the cluster stars used for the calibration (see Paper II). The dashed part is the region in which the calibration is extrapolated. Distances from the SMC optical center are given in the bottom right corner. The innermost field is on the left and the outermost one is on the right.

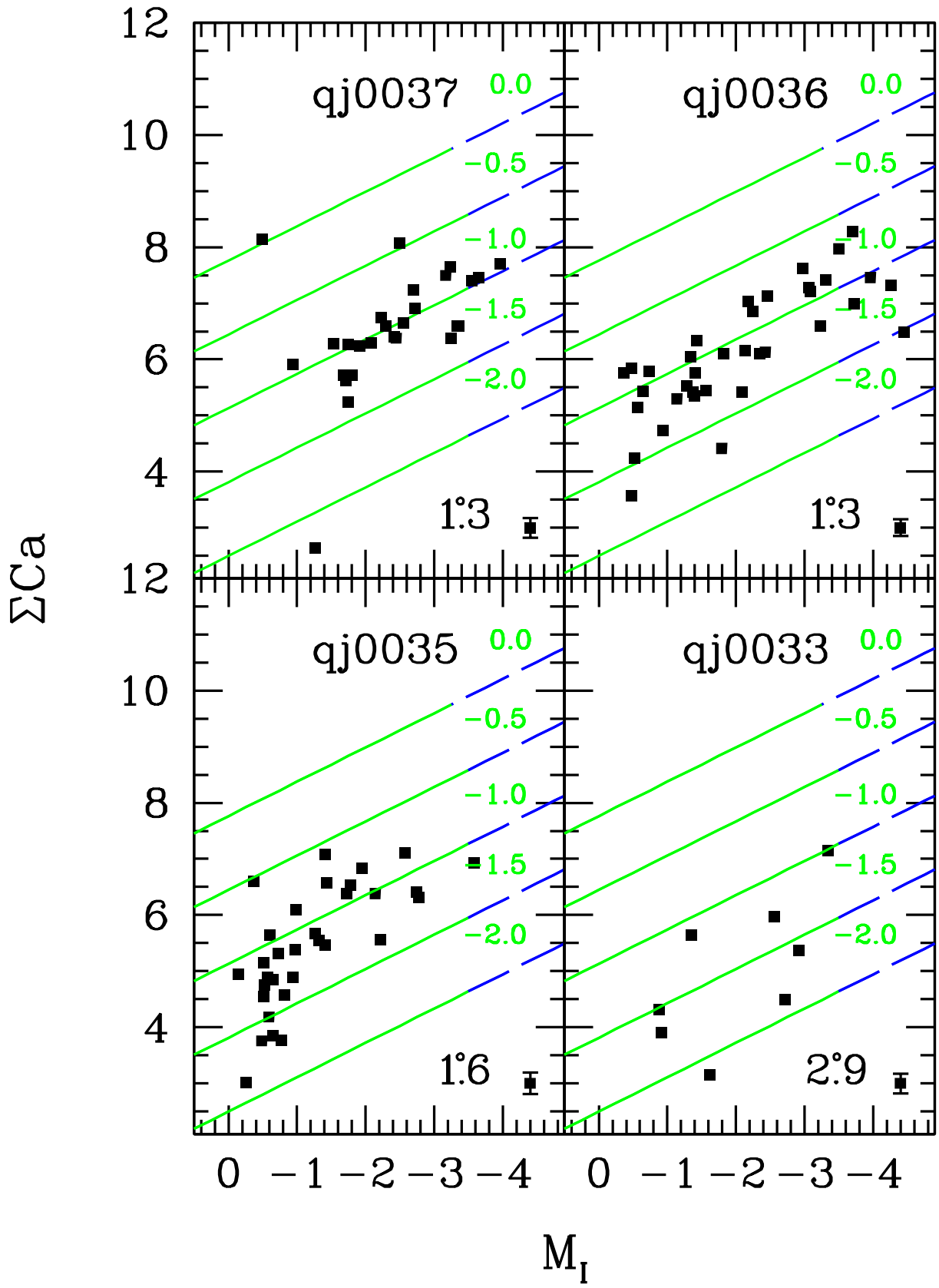

Fig. 3.— The same as Figure 2, for the Western fields. They are ordered from the innermost field (*top left*), to the outermost one (*bottom right*).

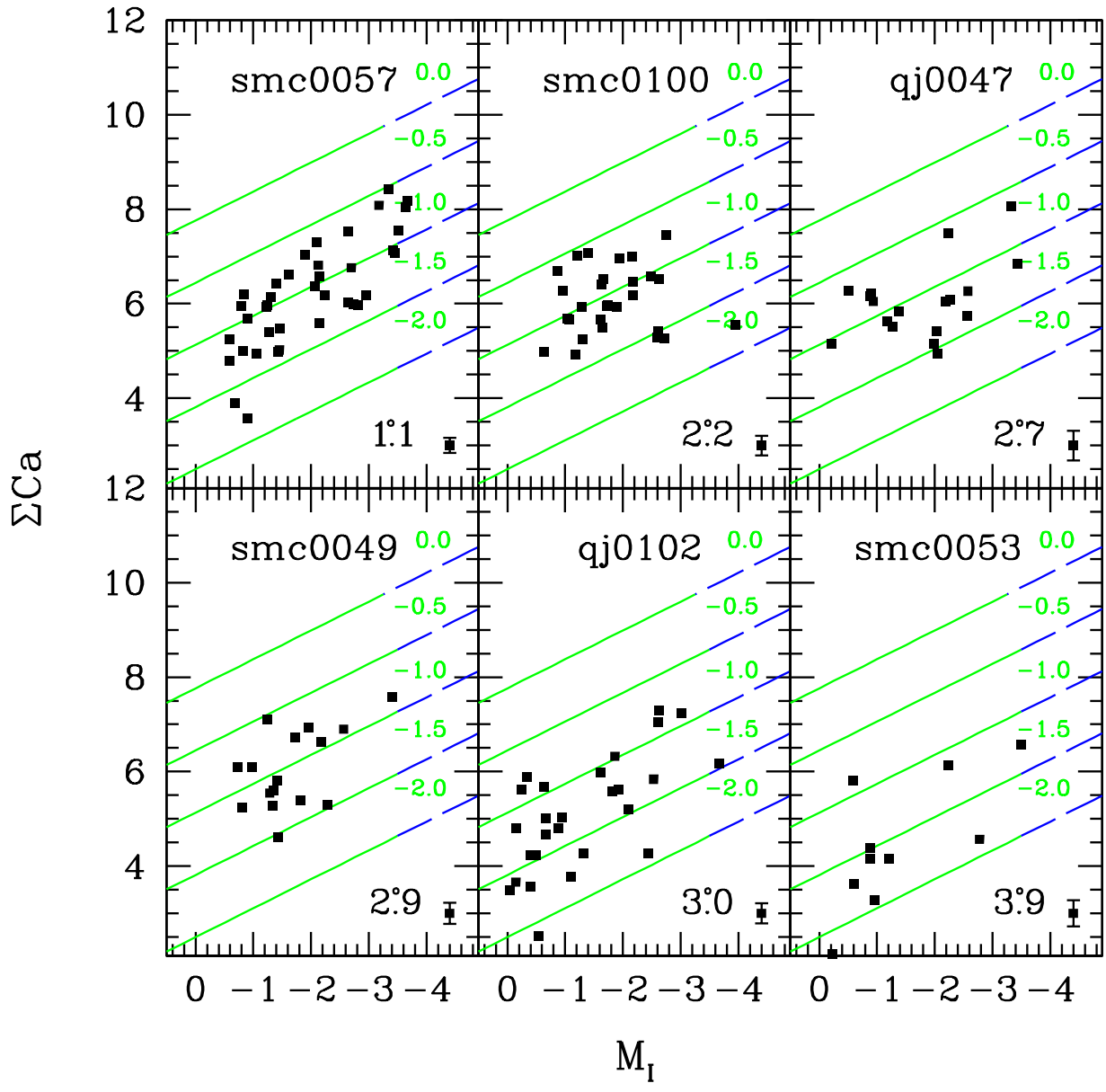

Fig. 4.— The same as Figure 2, for the Southern fields. They are ordered from the innermost field (*top left*), to the outermost one (*bottom right*).

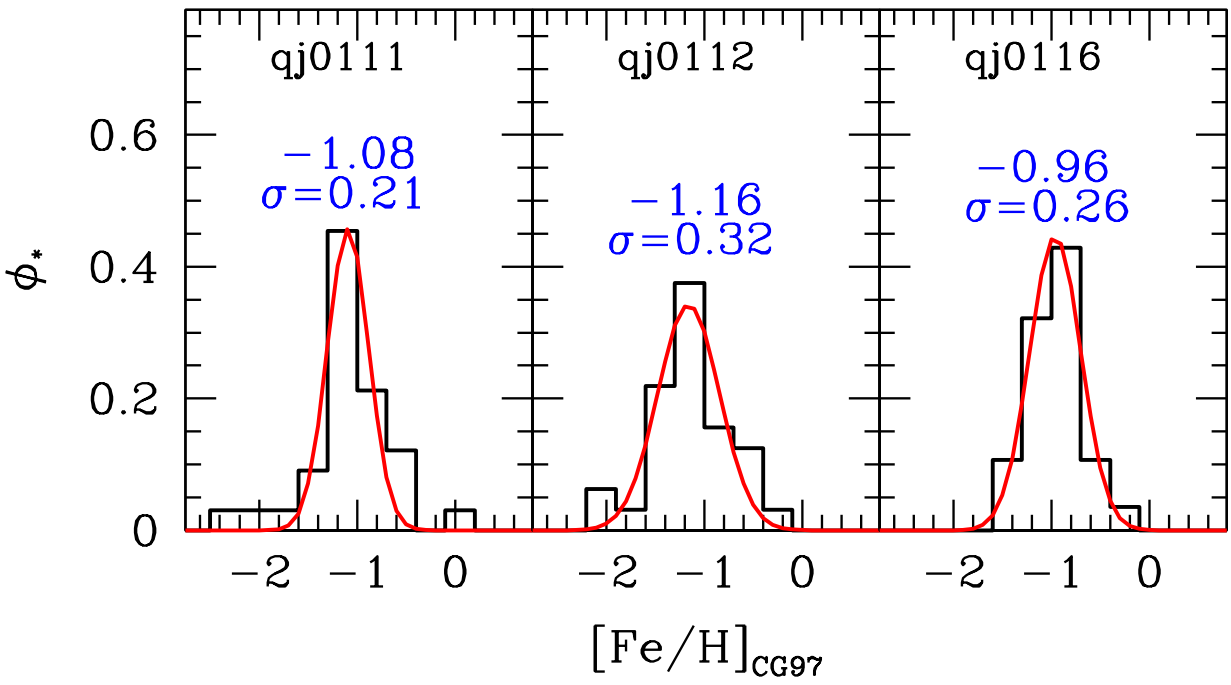

Fig. 5.— Metallicity distributions for the eastern fields in our sample. A Gaussian has been fitted to each distribution in order to obtain its mean and dispersion. The values obtained are shown in each panel.

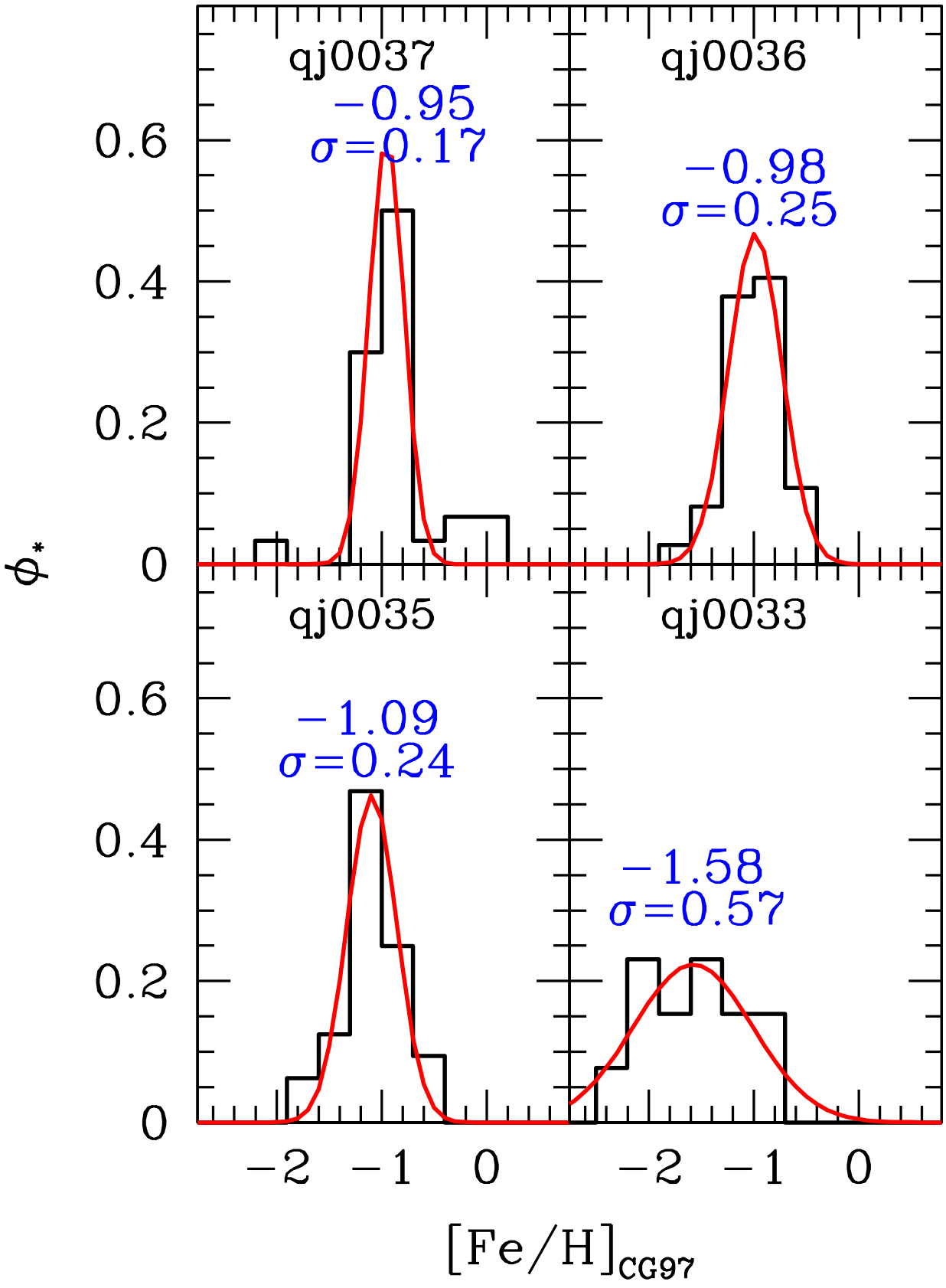

Fig. 6.— The same as Figure 5 for the western fields.

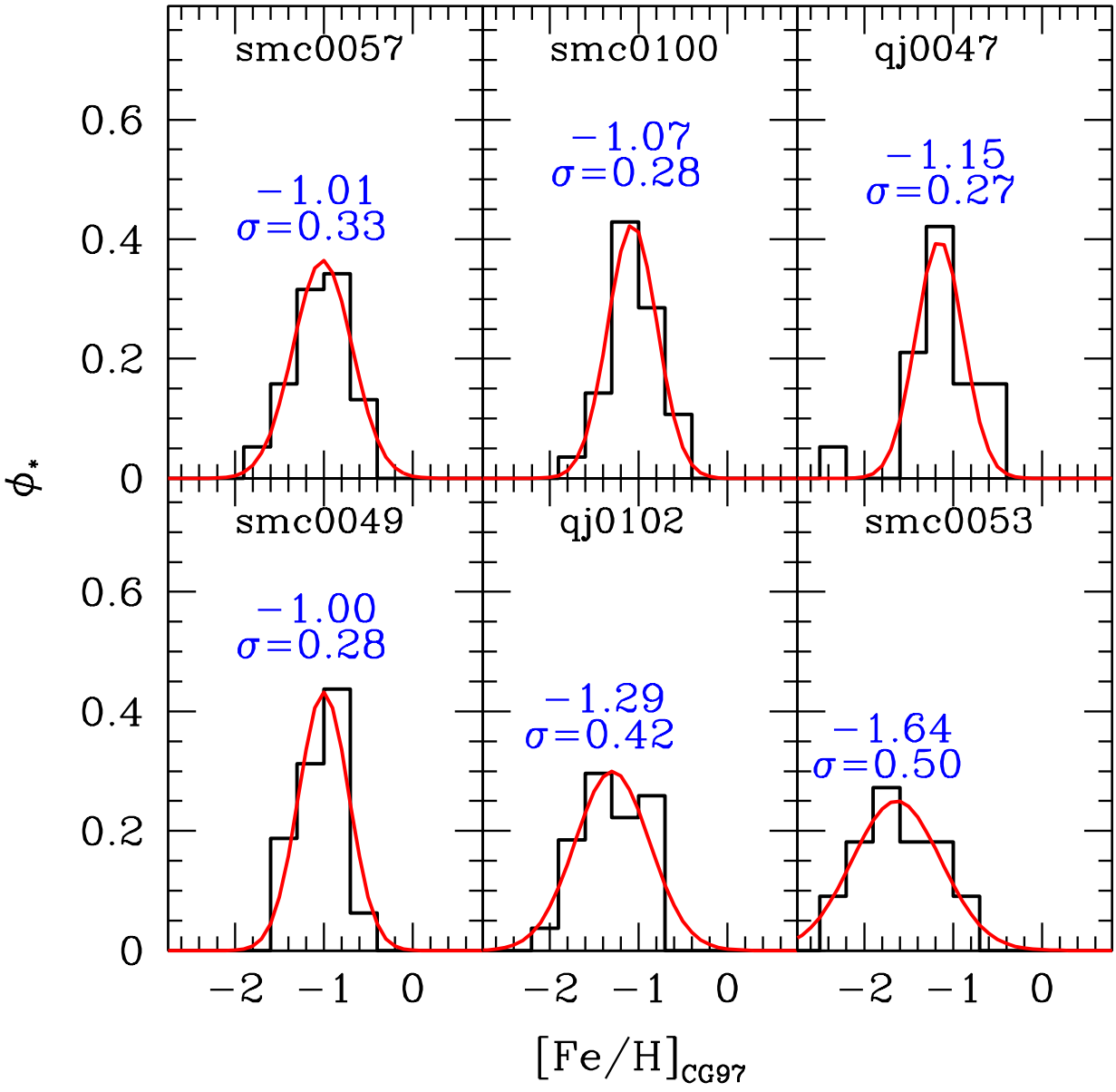

Fig. 7.— The same as Figure 5 for the southern fields.

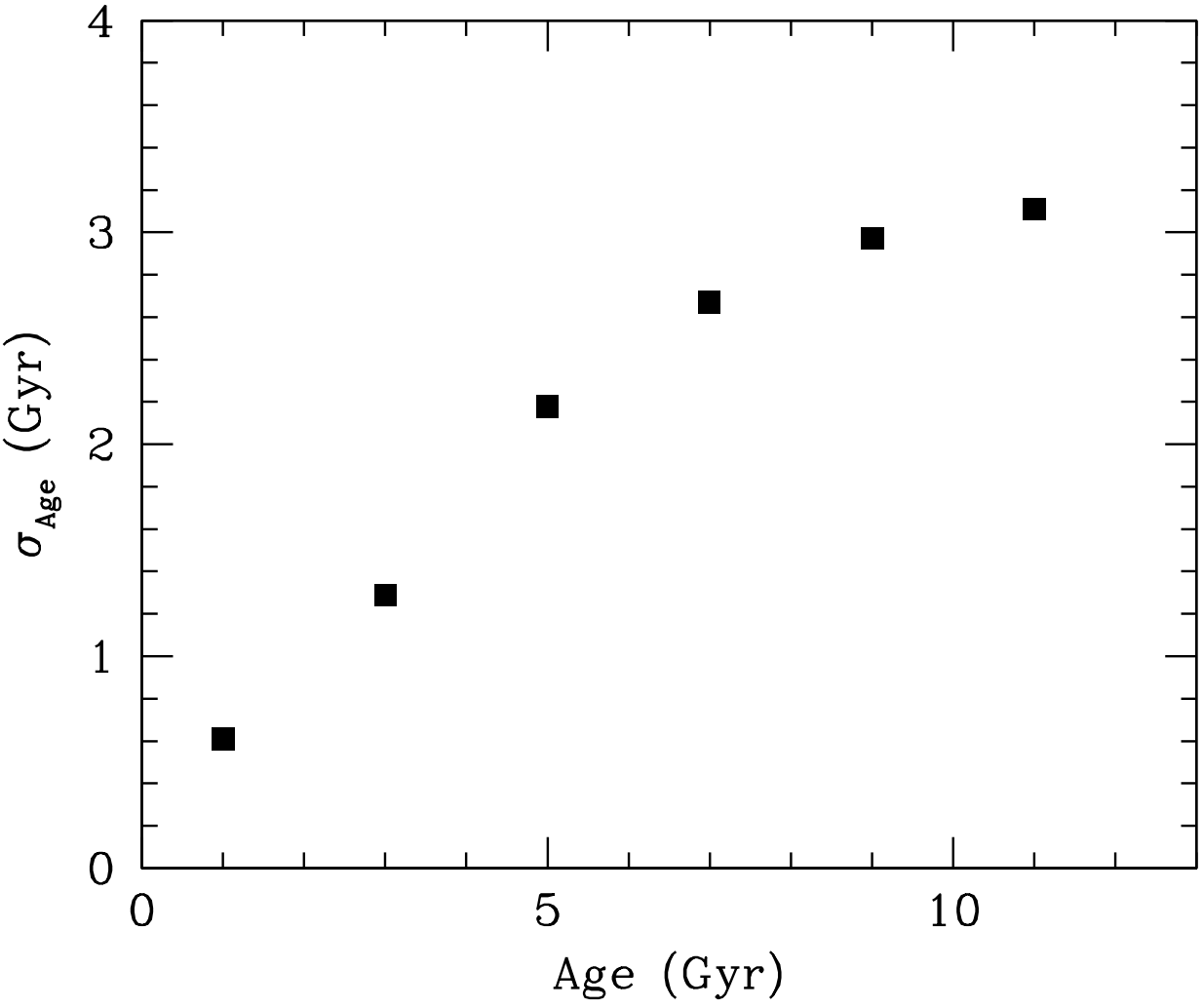

Fig. 8.— Age uncertainty as a function of age as calculated through a Monte Carlo test and using equation 2. See text for details.

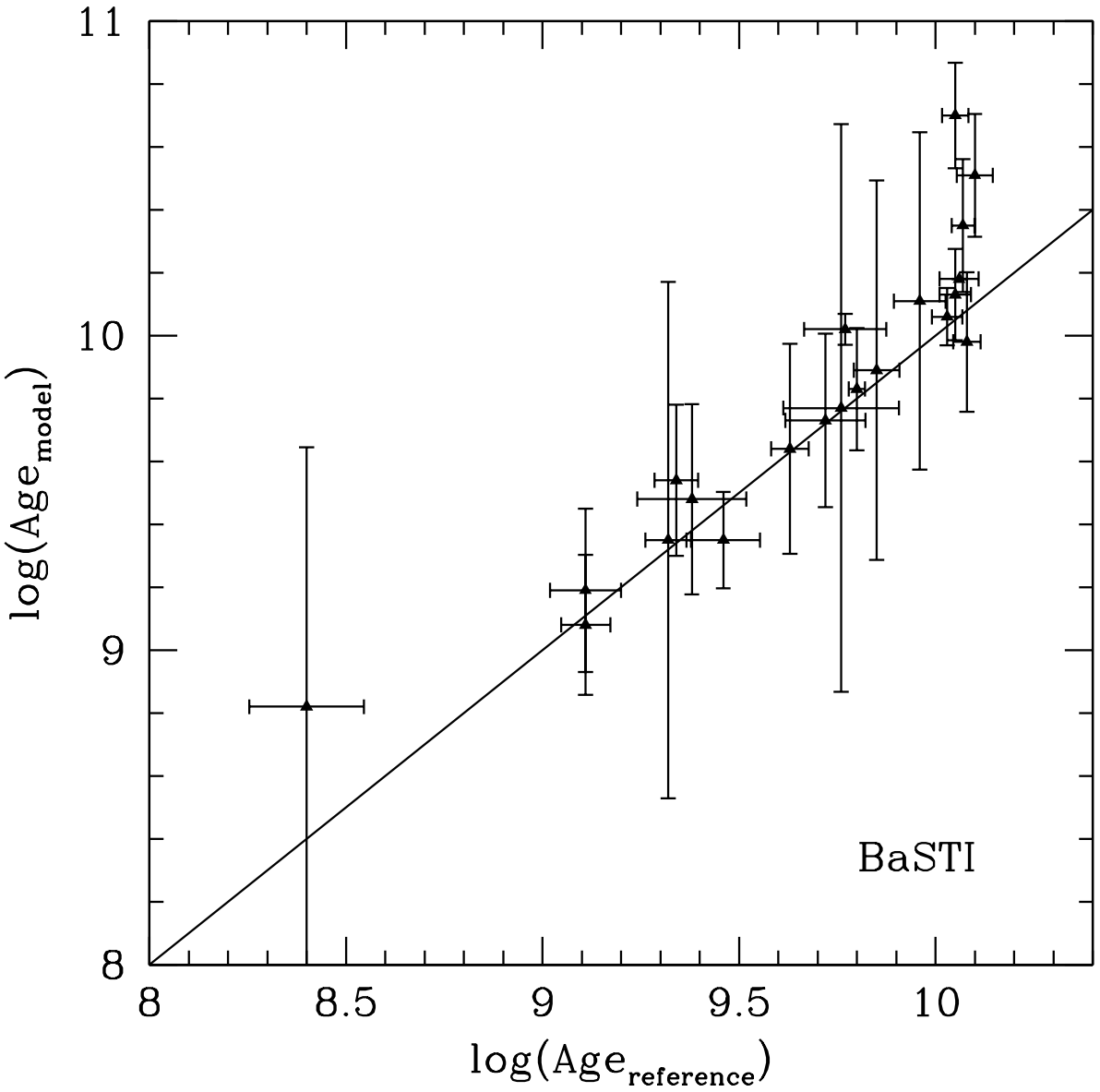

Fig. 9.— Ages derived from equation 2 for the cluster sample presented in Paper II, plotted against the reference values. The solid line corresponds to the one-to-one relation.

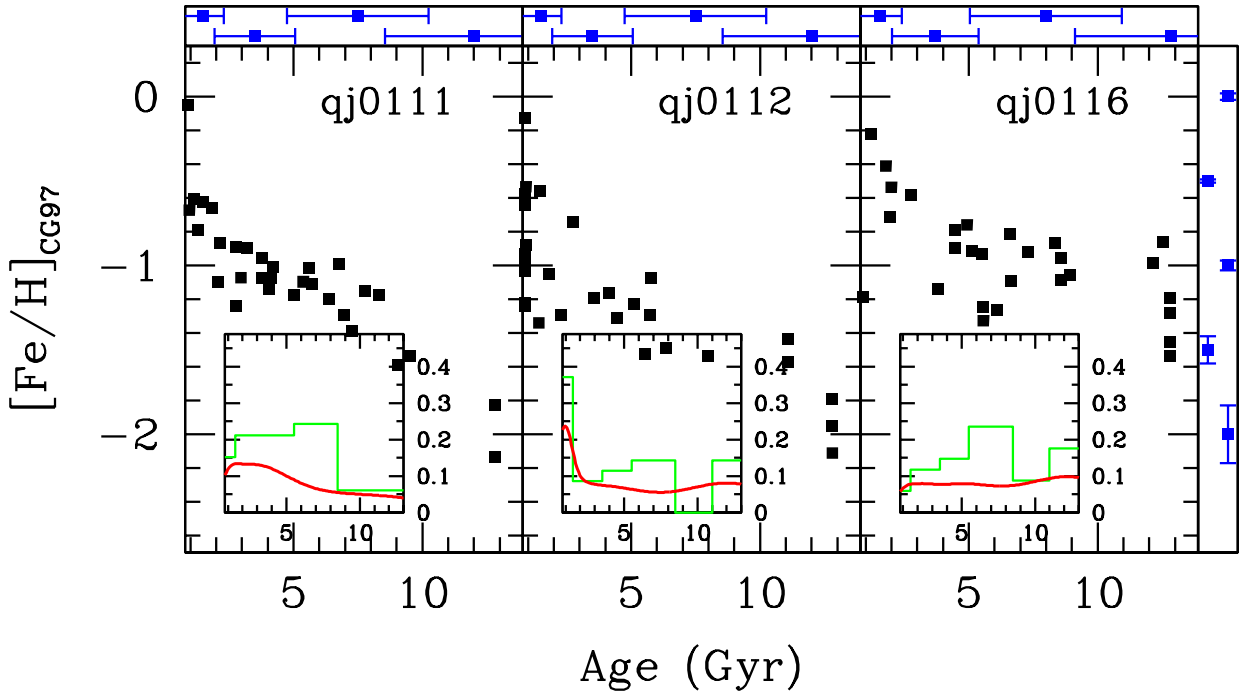

Fig. 10.— Age–metallicity relationships for the eastern SMC fields in our sample. Inset panels show the age distribution computed taking (*solid line*) and not taking (*histogram*) into account the age determination uncertainties. Top panels show the age error in each age interval (see Figure 8). Right panel shows the metallicity uncertainty in each metallicity bin.

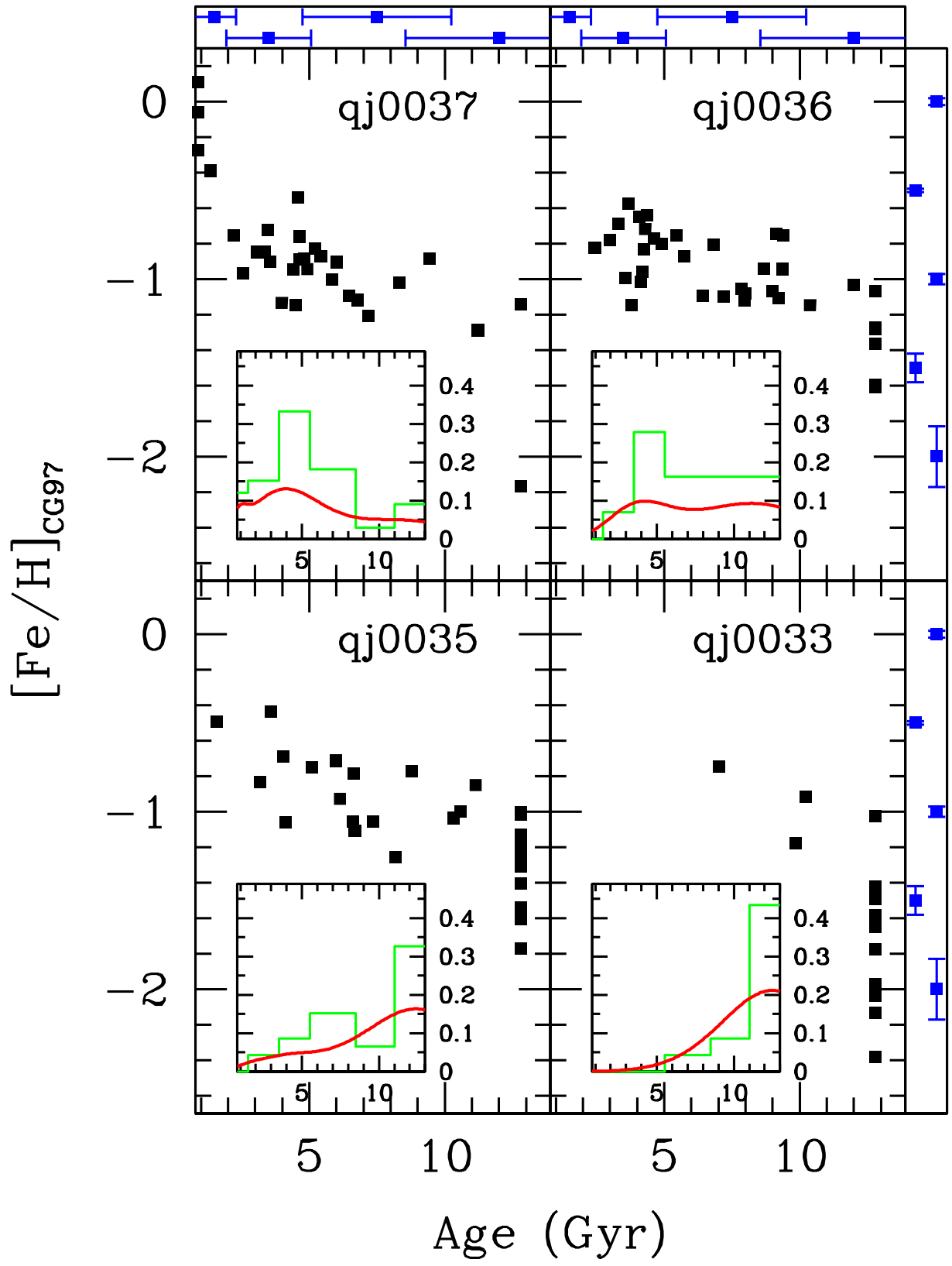

Fig. 11.— The same as Figure 10, for the western fields.

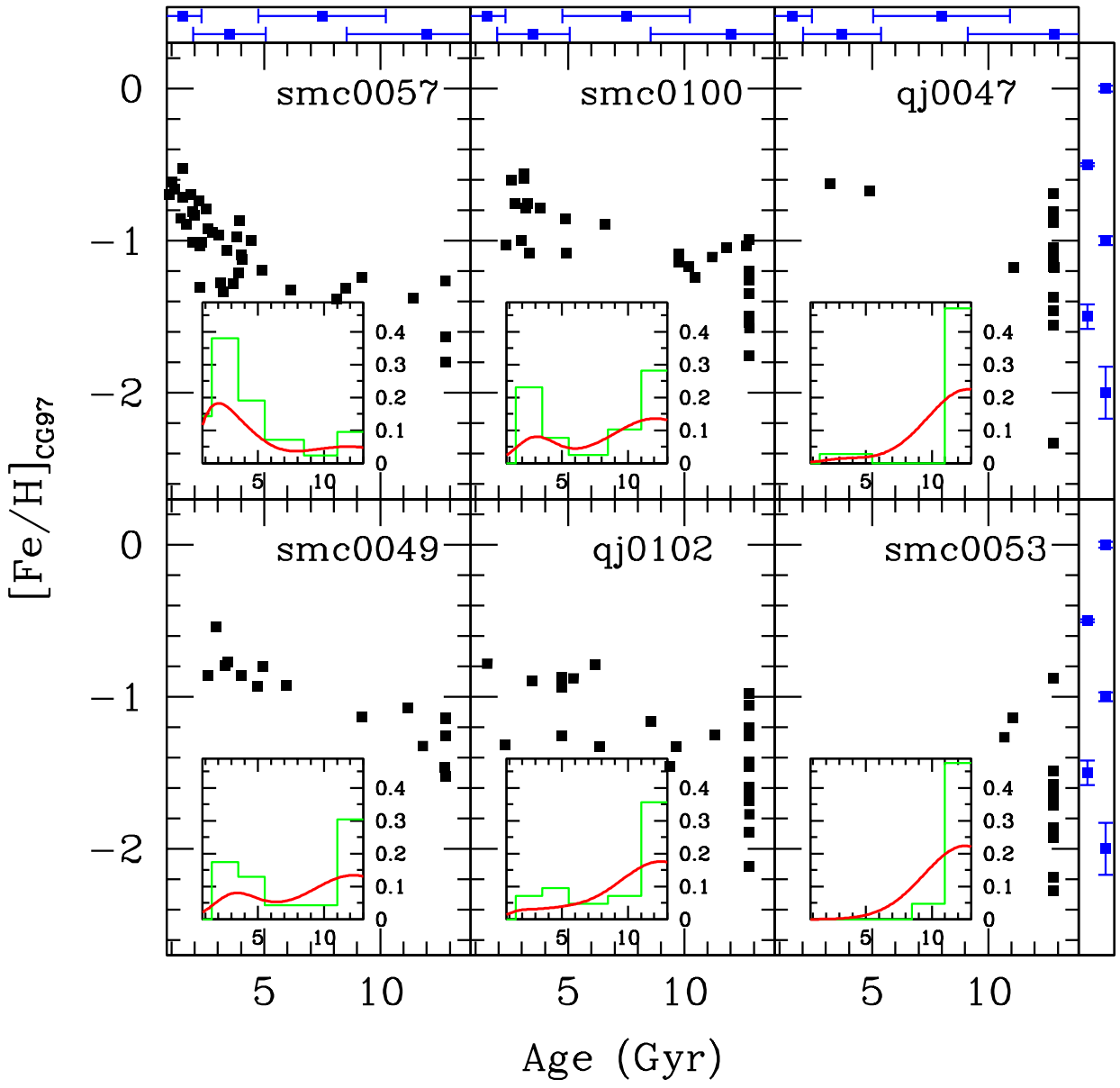

Fig. 12.— The same as Figure 10, for the southern fields.

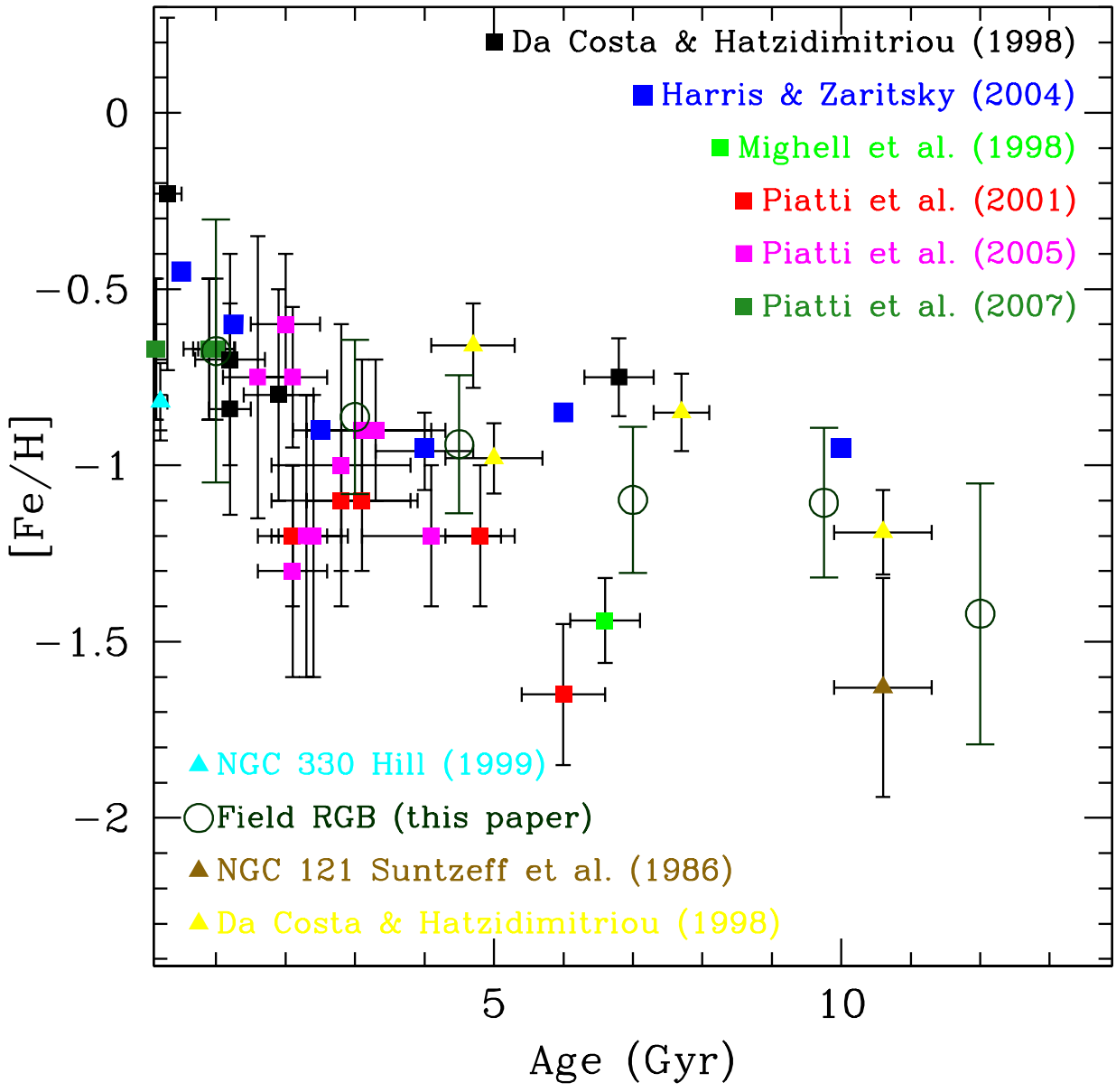

Fig. 13.— AMR for SMC clusters. Squares represent photometric determinations: M98: Mighell, Sarajedini, & French (1998, *green*); (Da Costa & Hatzidimitriou 1998, DH98, *black*); Piatti et al. (2001, P01, *red*); Piatti et al. (2005, P05, *pink*) and Piatti et al. (2007, P07, *dark green*). Triangles are spectroscopic determinations: NGC 121: **?**, S86, *brown*; Da Costa & Hatzidimitriou (1998, DH98, *yellow*) and NGC 330: Hill (1999, H99, *cyan*). Blue squares represent the AMR obtained from UBVI photometry by Harris & Zaritsky (2004, HZ04) in the central region of the galaxy. The mean metallicity in six age bins of our global SMC AMR has also been plotted (*open circles*). Note that the metallicity scales of each work may not be exactly the same.

Table 1. SMC observed fields

Field	α_{2000}	δ_{2000}	r(')	PA (°)	Zone	E(B-V)
smc0057	*00:57*	*-73:53*	*65.7*	*164.4*	*South*	*0.09*
qj0037	**00:37**	**-72:18**	**78.5**	**294.0**	**West**	**0.07**
qj0036	**00:36**	**-72:25**	**79.8**	**288.0**	**West**	**0.07**
*q*j0111	*0*1:11	-72:49	*8*0.9	*8*9.5	*E*ast	*0.*09
*q*j0112	*0*1:12	-72:36	*8*7.4	*8*1.0	*E*ast	*0.*09
qj0035	**00:35**	**-72:01**	**95.5**	**300.6**	**West**	**0.05**
*q*j0116	*0*1:16	-72:59	*1*02.5	*9*5.2	*E*ast	*0.*08
smc0100	*01:00*	*-74:57*	*130.4*	*167.5*	*South*	*0.05*
qj0047	*00:47*	*-75:30*	*161.7*	*187.7*	*South*	*0.05*
qj0033	**00:33**	**-70:28**	**172.9**	**325.0**	**West**	**0.03**
smc0049	*00:49*	*-75:44*	*174.8*	*184.6*	*South*	*0.06*
qj0102	*01:02*	*-74:46*	*179.5*	*169.4*	*South*	*0.05*
smc0053	*00:53*	*-76:46*	*236.3*	*179.4*	*South*	*0.06*

Table 2. Red giants stars observed

α_{2000}	δ_{2000}	Σ Ca	$\sigma_{\Sigma Ca}$	B	I	$V_r(kms^{-1})$	Comments	
00:33:53.8	-70:24:31.3	2.75	0.23	20.26	18.45	-307.1	68.5	No member
00:34:00.0	-70:28:22.9	2.56	0.42	20.31	18.57	79.0	4.2	
00:34:03.1	-70:27:07.7	1.89	0.71	20.82	18.97	78.9	3.3	
00:34:25.9	-70:27:47.1	5.64	0.19	19.66	17.61	133.5	3.7	
00:34:06.4	-70:27:39.3	1.95	0.12	18.67	17.81	162.2	2.9	
00:33:37.1	-70:27:31.8	5.10	0.08	18.82	15.82	69.9	3.1	
00:33:41.8	-70:27:14.3	5.17	0.20	19.72	17.46	31.7	2.9	No member

Note. — Table 2 is published in its entirety in the electronic edition of Astronomical Journal. A portion is shown here for guidance regarding its form and content

Table 3. Line and continuum bandpasses

Line Bandpasses (Å)	Continuum bandpasses (Å)
8484-8513	8474-8484
8522-8562	8563-8577
8642-8682	8619-8642
...	8799-8725
...	8776-8792

Table 4. Coefficients of the fit of equation 2 for BaSTI stellar evolution models (Pietrinferni et al. 2004). The fit standard deviation of the fit (σ) is shown in the last column.

a	b	c	d	e	f	σ
4.06±0.03	3.58±0.02	0.663±0.003	-1.314±0.006	-0.402±0.002	-0.077±0.005	0.40

Table 5. Metallicity distribution in each field.

Field	r(')	$\langle [Fe/H] \rangle$	$\sigma_{[Fe/H]}$	[Fe/H]<-1	[Fe/H]>-1.0
smc0057	*1.1*	*-1.01*	*0.33*	*53*	*47*
qj0037	**1.3**	**-0.95**	**0.17**	**35**	**65**
qj0036	**1.3**	**-0.98**	**0.25**	**49**	**51**
*qj*0111	*1.3*	-1.08	*0.2*1	*64*	*36*
*qj*0112	*1.4*	-1.16	*0.3*2	*69*	*31*
qj0035	**1.6**	**-1.09**	**0.24**	**66**	**34**
*qj*0116	*1.7*	-0.96	*0.2*6	*43*	*57*
smc0100	*2.2*	*-1.07*	*0.28*	*61*	*39*
qj0047	*2.7*	*-1.15*	*0.27*	*68*	*32*
qj0033	**2.9**	**-1.58**	**0.57**	**85**	**15**
smc0049	*2.9*	*-1.00*	*0.28*	*53*	*47*
qj0102	*3.0*	*-1.29*	*0.42*	*74*	*26*
smc0053	*3.9*	*-1.64*	*0.50*	*92*	*8*

Table 6. Average metallicity in six age bins. Also listed are the values obtained from the combination of the 13 fields. The last column shows the value χ^2_ν obtained from the comparison of each field with the global one.

Field	$\langle [Fe/H]_{\leq 1.5} \rangle$	$\langle [Fe/H]_{1.5-3.5} \rangle$	$\langle [Fe/H]_{3.5-5.5} \rangle$	$\langle [Fe/H]_{5.5-8.5} \rangle$	$\langle [Fe/H]_{8.5-11} \rangle$	$\langle [Fe/H]_{\geq 11} \rangle$	χ^2
smc0057	-0.68±0.11	-0.98±0.20	-1.09±0.14	-1.34±0.04	-1.24±0.05	-1.52±0.24	0.39
qj0037	-0.15±0.22	-0.83±0.10	-0.89±0.17	-1.06±0.11	-0.89±0.02	-1.53±0.55	0.44
qj0036	···	-0.76±0.07	-0.82±0.17	-1.01±0.12	-0.96±0.16	-1.32±0.23	0.17
*qj*0111	-0.55±0.29	-0.96±0.19	-1.07±0.07	-1.17±0.13	-1.56±0.04	-1.98±0.22	0.62
*qj*0112	-0.85±0.34	-1.03±0.28	-1.23±0.06	-1.38±0.20	···	-1.77±0.27	0.76
qj0035	···	-0.66±0.24	-0.73±0.26	-0.98±0.19	-0.94±0.14	-1.27±0.26	0.47
*qj*0116	-0.71±0.68	-0.56±0.12	-0.90±0.15	-1.06±0.20	-1.03±0.07	-1.22±0.26	0.30
smc0100	···	-0.80±0.20	-0.91±0.16	-0.89±0.02	-1.16±0.06	-1.30±0.26	0.24
qj0047	···	-0.63±0.01	-0.67±0.01	···	···	-1.20±0.38	1.07
qj0033	···	···	···	-0.74±0.01	-1.05±0.18	-1.75±0.40	1.07
smc0049	···	-0.74±0.14	-0.87±0.06	-0.92±0.02	-1.13±0.04	-1.28±0.17	0.24
qj0102	···	-1.00±0.28	-0.99±0.18	-1.06±0.38	-1.31±0.15	-1.49±0.31	0.17
smc0053	···	···	···	···	-1.27±0.05	-1.67±0.43	0.36
Global	-0.68±0.37	-0.86±0.22	-0.94±0.20	-1.10±0.21	-1.11±0.21	-1.42±0.37	···